

## Bandgap capability of hybrid Kirigami inspired cellular structures

S. Del Broccolo<sup>\*1,2</sup>, M. Ouisse<sup>1</sup>, E. Foltete<sup>1</sup> and F. Scarpa<sup>2</sup>

<sup>1</sup>Department of Applied Mechanics, University of Burgundy - Franche-Comté - FEMTO-ST – Institute  
CNRS/UFC/ENSMM/UTBM, 25000 Besançon, France

<sup>2</sup>Bristol Composites Institute (ACCIS), University of Bristol  
Queen's Building, University Walk, Bristol BS8 1TR, U.K.

(Received September 14, 2018, Revised February 26, 2019, Accepted March 19, 2019)

**Abstract.** Periodic cellular core structures included in sandwich panels possess good stiffness while saving weight and only lately their potential to act as passive vibration filters is increasingly being studied. Classical homogeneous honeycombs show poor vibroacoustic performance and only by varying certain geometrical features, a shift and/or variation in bandgap frequency range occurs. This work aims to investigate the vibration filtering properties of the AUXHEX “hybrid” core, which is a cellular structure containing cells of different shapes. Numerical simulations are carried out using two different approaches. The first technique used is the harmonic analysis with commercially available software, and the second one, which has been proved to be computationally more efficient, consists in the Wave Finite Element Method (WFEM), which still makes use of finite elements (FEM) packages, but instead of working with large models, it exploits the periodicity of the structure by analysing only the unit cell, thanks to the Floquet-Bloch theorem. Both techniques allow to produce graphs such as frequency response plots (FRF's) and dispersion curves, which are powerful tools used to identify the spectral bandgap signature of the considered structure. The hybrid cellular core pattern AUXHEX is analysed and results are discussed, focusing the investigation on the possible spectral bandgap signature heritage that a hybrid core experiences from their “parents” homogeneous cell cores.

**Keywords:** WFEM ; periodic media ; bandgaps ; Transfer matrix method ; cellular structures

### 1. Introduction

Today, there are many examples of periodic structures in the engineering domain. Stiffened plates, train rails, bridges, skyscrapers, space launchers as well as composites sandwich panels are just few examples. Due to the solicitations experienced, the study of wave propagation within such structures as well as understanding their dynamic behavior, is important to avoid catastrophic failures and to lengthen the average service lifespan.

Honeycomb sandwich panels are well known to provide interesting static out of plane properties (compression) because of their high equivalent stiffness whilst containing mass. However, this makes such structures possess a very high stiffness/mass ratio and therefore, their vibration frequency domain is usually in the high range. Aerospace, automotive and naval

---

\*Corresponding author, Ph.D., E-mail: [simone.delbroccolo@femto-st.fr](mailto:simone.delbroccolo@femto-st.fr)

industries all have the preference of obtaining lightweight structures and this makes sandwich panels very attractive, but at the same time, the frequencies to be dealt with in these operating environments are in the mid-low range. As engineered today, (concentrating only on static aspects) the periodicity of such structures is not fully exploited. Obtaining sandwich panels with improved vibroacoustic performances at specific frequencies is therefore an interesting research topic.

The response of periodic structures to external excitation has already been investigated starting from Brillouin's work back in 1946. Mead *et al.* (1996) have produced a document, summarizing almost thirty years of work carried out at the University of Southampton, demonstrating how spatial periodicity in terms of structure, material or boundary layers, is detected by a travelling wave as a discontinuity point in the medium. Those periodic variations cause some of the incident waves to be reflected and some to be transmitted. The destructive interaction between incident and reflected waves causes attenuation (bandgaps) at certain frequency ranges, and therefore, periodic structures can act as passive filters. This intuitively brings the reader to reasonably think that there is a relation between the geometrical dimensions of the periodic structure and the travelling wave direction and characteristics. Each periodic structure possesses natural bandgaps that depend upon the geometry and those are defined as Bragg bandgaps.

Different methods that have been developed in the years to analyse periodic structures and most of them can be found in literature. A good summary of those techniques which mostly are FEM derived can be found in the paper written by Hussein and Ruzzene (2014).

The most commonly used one lately is the Wave Finite Element Method (WFEM). The mass and stiffness matrices of the unit cell are extracted with FEM commercial software and used to calculate the dynamics of the structure by applying the Floquet-Bloch periodicity conditions.

A previous work by Del Broccolo *et al.* (2017), attempted to produce, successfully, a cellular structure possessing zero in-plane Poisson's coefficient. This was obtained using a hybrid tessellation which conferred the overall structure, the desired property. By hybrid, is intend a cellular core containing cells of different shapes. This was achieved using PEEK thermoplastic thin sheets and the Japanese art technique of cutting and folding paper, known as Kirigami. Whilst the static properties have already been investigated, the vibration filtering properties of the hybrid pattern named AUXHEX have not yet been covered, although F. Scarpa *et al.* (2003) were, to the authors' knowledge, the first ones to investigate wave propagation in a Kirigami lattice. In this work, numerical simulations are carried out with the aim of investigating the vibration filtering properties of such structure using two different approaches (finite FRF and infinite structure 1D WFEM) and software like ANSYS and MATLAB.

The main indicator to evaluate the vibroacoustic performance of the AUXHEX hybrid core, will be the number and range of stopbands that the structure possesses. Additionally, two classic tessellations, hexagonal and re-entrant will also be analysed and used as reference.

An overview of the investigation methods as well as some considerations on the results obtained are proposed.

## 2. Wave propagation in periodic media

### 2.1 Periodic structures

It is defined as periodic, a structure which exhibits some form of spatial periodicity. Such characteristic can be in its constituent material, internal geometry or the boundary conditions. This periodic feature gives the possibility to do considerations about the behavior of the full structure

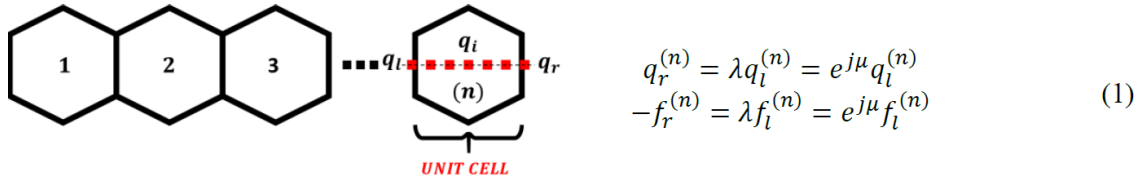


Fig.1 Periodic structure unit cell

by carrying out analyses on just a portion of structure as shown by B. R. Mace *et al.* 2005 and F. Scarpa *et al.* (2013). The portion that enables us to recreate the full structure by repeating itself is usually called unit cell.

### 2.2 Floquet-Bloch Theory (indirect method)

This theory is the core of the WFEM method and was firstly introduced for engineering investigations by Brillouin (1953). According to this theory, displacements and forces on the nodes on the extremities of a unit cell are related. This means that it is enough to analyse a small portion of the periodic structure to understand the overall dynamic behavior.

In Fig.1, the Floquet-Bloch relation is shown, where  $\mu = kL$  is the reduced wave number,  $k$  is the wave number and  $L$  the length of the unit cell.

To understand the dynamic behavior of a periodic structure, a dispersion curve, which represents the relation between the reduced wavenumber  $\mu$  versus the frequency  $\omega$  can be plotted. To produce a dispersion curve therefore, a relation between  $\omega$  and  $\lambda = e^{j\mu}$  is required. The starting point is represented by the Fundamental Dynamics Equation of the unit cell below

$$(K_{uc} - \omega^2 M_{uc}) \begin{pmatrix} q_l \\ q_i \\ q_r \end{pmatrix} = \begin{pmatrix} f_l \\ f_i \\ f_r \end{pmatrix} \tag{2}$$

where  $K_{uc} = \begin{bmatrix} K_{LL} & K_{LI} & K_{LR} \\ K_{IL} & K_{II} & K_{IR} \\ K_{RL} & K_{RI} & K_{RR} \end{bmatrix}$  and  $M_{uc} = \begin{bmatrix} M_{LL} & M_{LI} & M_{LR} \\ M_{IL} & M_{II} & M_{IR} \\ M_{RL} & M_{RI} & M_{RR} \end{bmatrix}$  are the stiffness and the mass matrix of the unit cell, and the objective is to convert this relation into an eigenvalue problem, by cancelling the force vector on the right-hand side.

By applying the Floquet-Bloch conditions on forces and displacements into Eq. (2), the following is obtained

$$q = \begin{pmatrix} q_l \\ q_i \\ q_r \end{pmatrix} = \begin{pmatrix} q_l \\ q_i \\ \lambda q_l \end{pmatrix} = \Lambda_R \begin{pmatrix} q_l \\ q_i \end{pmatrix} \tag{3}$$

where,  $\Lambda_R = \begin{bmatrix} I & 0 \\ 0 & I \\ \lambda I & 0 \end{bmatrix}$

For the forces, focus is on the RHS of Equation (1) and  $f_i = 0$  is also assumed

$$f = \begin{pmatrix} f_l \\ f_i \\ f_r \end{pmatrix} = \begin{pmatrix} f_l \\ 0 \\ f_r \end{pmatrix} \tag{4}$$

$$\text{Let } \Lambda_L = \begin{bmatrix} I & 0 & \frac{1}{\lambda}I \\ 0 & I & 0 \end{bmatrix}$$

By pre-multiplying  $f$  by  $\Lambda_L$  the following is obtained due to Floquet-Bloch theory

$$\Lambda_L \begin{pmatrix} f_l \\ 0 \\ f_r \end{pmatrix} = \begin{bmatrix} I & 0 & \frac{1}{\lambda}I \\ 0 & I & 0 \end{bmatrix} \begin{pmatrix} f_l \\ 0 \\ f_r \end{pmatrix} = \begin{pmatrix} f_l + \frac{1}{\lambda}f_r \\ 0 \end{pmatrix} = 0 \quad (5)$$

Substituting those two conditions into Equation (1), still assuming that  $f_l = 0$ : obtaining the equation that describes the dynamics of the unit cell

$$\Lambda_L(K_{uc} - \omega^2 M_{uc}) \begin{pmatrix} q_l \\ q_i \\ q_r \end{pmatrix} = \Lambda_L \begin{pmatrix} f_l \\ 0 \\ f_r \end{pmatrix} \quad (6)$$

$$\Lambda_L(K_{uc} - \omega^2 M_{uc}) \begin{pmatrix} q_l \\ q_i \\ q_r \end{pmatrix} = 0$$

The RHS of equation (6) is equal to zero thanks to the Floquet-Bloch relation just derived. By applying the condition on the displacements to Eq. (2) obtaining

$$\begin{aligned} \Lambda_L(K_{uc} - \omega^2 M_{uc})\Lambda_R \begin{pmatrix} q_l \\ q_i \end{pmatrix} &= 0 \\ (\Lambda_L K_{uc} \Lambda_R - \omega^2 \Lambda_L M_{uc} \Lambda_R) \begin{pmatrix} q_l \\ q_i \end{pmatrix} &= 0 \\ (K_r(\mu) - \omega^2 M_r(\mu))q^{(r)} &= 0 \end{aligned} \quad (7)$$

reaching finally this standard eigenvalue problem.

Solving for  $\mu \in [0; \pi]$  which represents the First Brillouin Zone, one can then obtain the frequency vector and plot the dispersion curve. The input value  $\mu$  though is a complex number where the real part describes the propagative waves while the imaginary part describes the evanescent ones. The range of the imaginary contribution, contrary to the real part, can assume any value and can't be predicted prior. Since the main interest is represented by the propagative waves, only  $\text{Re}(\mu)$  is injected, missing the imaginary contribution as a trade-off.

### 3. Investigation methods

As mentioned in the introduction, the objective is to perform vibration analyses on the AUXHEX topology to see whether it possesses better vibration filtering properties with respect to the classical regular hexagonal and re-entrant honeycombs, for the same frequency range. The parameter that will be taken into consideration to evaluate the topology performance is the number and width of bandgaps. The main questions to answer were the following:

- In certain frequency ranges, where and how many bandgaps can the topology produce?
- How does the change in certain geometrical parameters affect the bandgaps?
- The first question is answered comparing topologies keeping the relative density constant.
- The parametrical analysis instead is carried out by varying the aspect ratio between the length of the beam and the side of its square section.

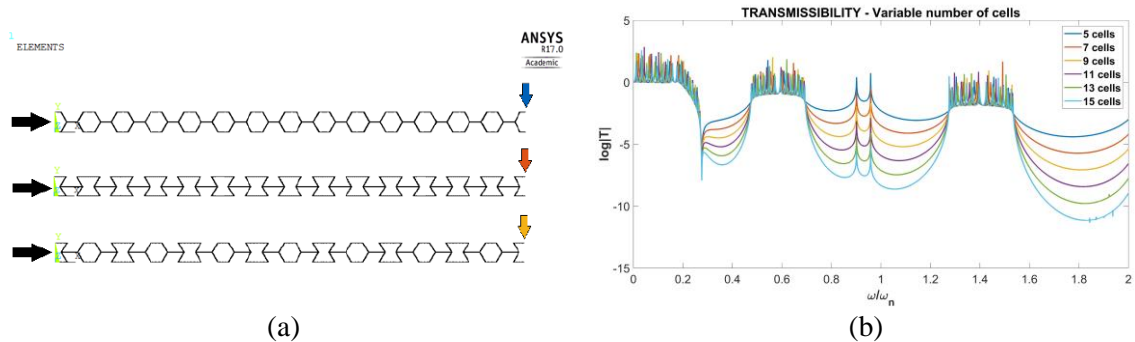


Fig. 2 (a) Analysed truss structures with input force (black arrows) and output readings (coloured arrows) and (b) In-plane compression 1D FRF for increasing number of cells

Two methods are used for each topology to cross check results and perform this topology comparison; they can be defined as finite and infinite structure approaches. Both make use of ANSYS APDL 18.1 FEA software. The first one is a Harmonic simulation with a finite structure, which was used to produce an FRF plot to illustrate the validity of the bandgap locations. The second one is a design tool which uses the Floquet Bloch theory and TMM to produce dispersion curves linking frequency with the reduced wave number. This method is implemented in MATLAB and before proceeding with the actual bandgap evaluation (over the selected frequency range), agreement between the bandgaps found using commercial software and the TMM will be verified.

### 3.1 Harmonic analysis

A compression force is applied at one end of a truss structure created with an array of twenty unit cells in the X direction. The displacement amplitude of the selected nodes at the extremities of the truss was extracted and used to plot FRF's. The same type of harmonic study was done by applying a bending (in-plane) force and recording the displacements in the Y direction. In both cases, only three degrees of freedom were allowed and those were UX, UY and ROT-Z.

The higher the number of cells, the higher the drop in correspondence of stopbands, as shown in Fig.2. This characteristic helped us identify which part of the plot corresponds to bandgaps.

### 3.2 Transfer matrix method (TMM)

To investigate the dynamic behavior of a periodic structure, a full-scale model can be produced, and through heavy calculation and therefore long computational time, the response of the structure is obtained. This translates in a very large number of nodes and therefore degrees of freedom that one needs to compute. Another way of doing it is by imposing the continuity and equilibrium relations at the interface of unit cells, and analysing the single unit cell instead of the full structure (reduced number of degrees of freedom to be considered). Those concepts can be used to obtain a method where forces and displacements at the extremities of the structure are related by a single matrix T which will have dimensions considerably reduced with respect to the full model. To link displacements and forces at the extremities of the unit cell, equation (2) is required neglecting damping.

According to the continuity of displacements and equilibrium of forces (Fig.3), relations (8) and (9) are derived which constitute the dynamic ligaments between the unit cells.

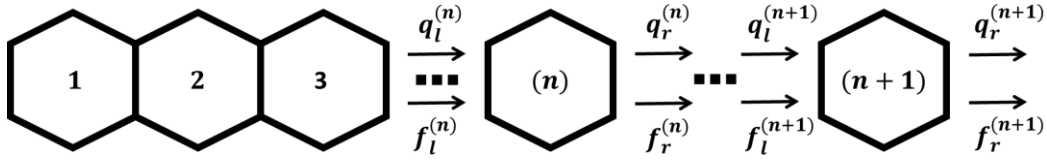


Fig. 3 Unit cell interactions

$$q_r^{(n)} = q_l^{(n+1)} \tag{8}$$

$$f_r^{(n)} = -f_l^{(n+1)} \tag{9}$$

For free wave propagation, no external forces act on the structure and the only ones considered are the ones at the interface between unit cells. The dynamic relation becomes

$$(K_{uc} - \omega^2 M_{uc}) \begin{pmatrix} q_l \\ q_r \end{pmatrix} = \begin{pmatrix} f_l \\ 0 \\ f_r \end{pmatrix} \tag{10}$$

$$D(\omega) \begin{pmatrix} q_l \\ q_r \end{pmatrix} = \begin{pmatrix} f_l \\ 0 \\ f_r \end{pmatrix} \tag{11}$$

where  $D(\omega) = \begin{bmatrix} D_{LL} & D_{LI} & D_{LR} \\ D_{IL} & D_{II} & D_{IR} \\ D_{RL} & D_{RI} & D_{RR} \end{bmatrix}$  is the *Dynamic matrix* which contains both mass and stiffness matrices of the unit cell and  $f_i = 0$ .

After a condensation procedure, the dynamic equation finally becomes

$$\begin{bmatrix} \tilde{D}_{LL} & \tilde{D}_{RL} \\ \tilde{D}_{LR} & \tilde{D}_{RR} \end{bmatrix} \begin{pmatrix} q_l \\ q_r \end{pmatrix} = \tilde{D}(\omega) \begin{pmatrix} q_l \\ q_r \end{pmatrix} = \begin{pmatrix} f_l \\ f_r \end{pmatrix} \tag{12}$$

$\tilde{D}(\omega)$  is the condensed dynamic matrix which possesses the following terms

$$\begin{aligned} \tilde{D}_{LL} &= D_{LL} - D_{LI} \times D_{II}^{-1} \times D_{IL} \\ \tilde{D}_{LR} &= D_{LR} - D_{LI} \times D_{II}^{-1} \times D_{IR} \\ \tilde{D}_{RL} &= D_{RL} - D_{RI} \times D_{II}^{-1} \times D_{IL} \\ \tilde{D}_{RR} &= D_{RR} - D_{RI} \times D_{II}^{-1} \times D_{IR} \end{aligned}$$

Now, by rearranging the items, the Transfer Matrix

$$\begin{pmatrix} q_r \\ -f_r \end{pmatrix} = \begin{bmatrix} T_{11} & T_{12} \\ T_{21} & T_{22} \end{bmatrix} \begin{pmatrix} q_l \\ f_l \end{pmatrix} = \mathbf{T} \begin{pmatrix} q_l \\ f_l \end{pmatrix} \tag{13}$$

$$T_{11} = -\tilde{D}_{LR}^{-1} \times \tilde{D}_{LL}$$

$$T_{21} = -\tilde{D}_{RL} + \tilde{D}_{RR} \times \tilde{D}_{LR}^{-1} \times \tilde{D}_{LL}$$

$$T_{12} = \tilde{D}_{LR}^{-1}$$

$$T_{22} = -\tilde{D}_{RR} \times \tilde{D}_{LR}^{-1}$$

The eigenvalues of  $T$ , correspond to the values of  $\lambda = e^{j\mu}$  and so, the response for an infinite structure can be plotted. One powerful characteristic of the matrix  $T$  is that is true for every

cell, so if dealing with a finite structure, a simple multiplication of it by itself will allow to link the first cell to the last one. For (n) cells therefore

$$\begin{pmatrix} q_r \\ -f_r \end{pmatrix}_{(n)} = T^n \begin{pmatrix} q_l \\ f_l \end{pmatrix}_{(1)} \quad (14)$$

Having frequency as the input, the reduced wave number  $\mu$  can be obtained, and the dispersion curves produced. The output using the direct approach, contrary to the indirect approach explained in section 2.2, produces both imaginary and real contributions of  $\mu$ . This information is useful because depending on the degrees of freedom of the model, the interpretation of the branches in the dispersion curves becomes easier because it allows to subdivide each branch with the type of travelling wave (in-plane compression or bending, out-of-plane bending, torsion).

#### 4. Numerical simulations

Here, the well-known harmonic approach is used in symbiosis with the novel WFEM. The latter is computationally favourable and is used to obtain the relation between frequency and reduced wave number, which is critical in describing the dynamic behaviour of the structure.

##### 4.1 Finite element model

In terms of FE modelling, ANSYS Mechanical APDL was used and the material properties (Biotex flax/PP natural fibre prepreg) used for the model are shown in Table 1.

Beam elements (BEAM 4) were used for both the Harmonic (finite approach) and the Substructure (used for infinite approach) analysis. In none of the cases damping was used.

##### 4.2 Core constant relative density

A first comparison between these topologies is carried out keeping constant the core relative density. In this way, the overall out of plane mechanical static compression properties as well as the overall weight of the core per unit area, are kept constant as described by Gibson in his book

Table 1 Biotex flax/pp material properties (thermoformed)

|                                      |            |
|--------------------------------------|------------|
| <i>Young's Modulus ,E [GPa]</i>      | <b>8.1</b> |
| <i>Density,ρ [kg m<sup>-3</sup>]</i> | 1040       |
| <i>Poisson's Ratio,ν</i>             | 0.2        |

Table 2 Unit cell parameters

| Topology   | <b>l</b> [mm] | <b>θ</b> [deg] | Rel. density | <b>(ω)</b> 1 <sup>st</sup> eigenfreq. [Hz] | <b>(2ω)</b> Freq. range [Hz] |
|------------|---------------|----------------|--------------|--|------------------------------|
| Hexagonal  | 5.499         | 30.00          | 0.042        | 8373                                       | 16746                        |
| Re-entrant | 7.331         | 30.00          | 0.042        | 4710                                       | 9420                         |
| AUXHEX     | 6.415         | 30.00          | 0.042        | 6152                                       | 12304                        |

about cellular solids [12]. This seemed a reasonable way of comparing different topologies isolating the vibration performance of the latter.

The relative density of the cellular structure is calculated as being the ratio between the volumes of the actual unit cell constituent material over the volume effectively occupied by it.

The harmonic response simulations were carried out without implementing any sort of damping in the structure. The plots show extremely high drops in amplitude to very large negative values. This must be physically interpreted as a bandgap region where none of the input

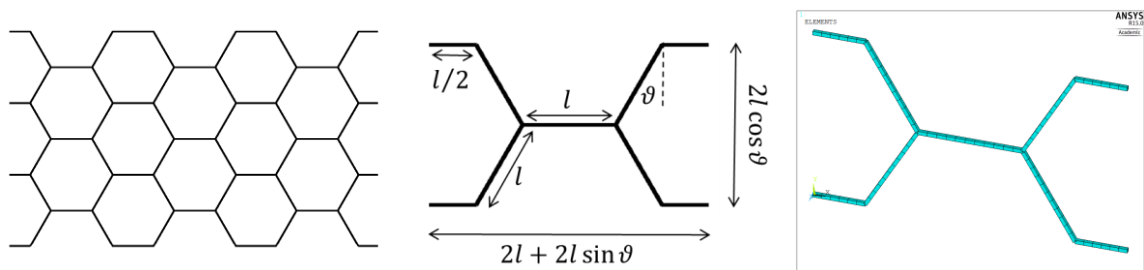


Fig. 4 Hexagonal unit cell (left) and example core (right)

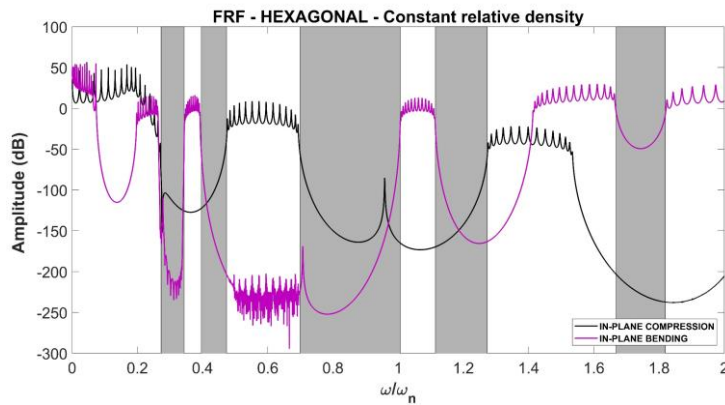


Fig. 5 FRF plot for Hexagonal topology

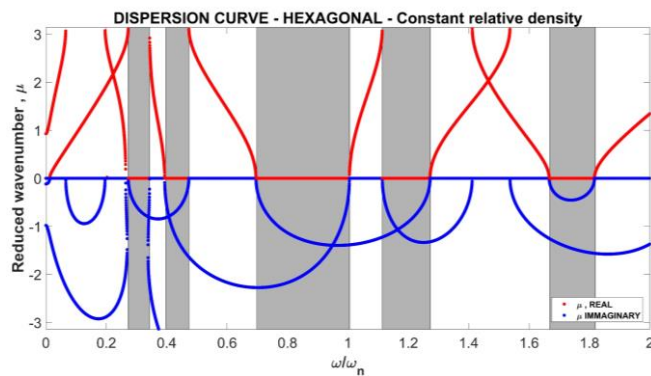


Fig. 6 Dispersion curve for Hexagonal topology

solicitation/displacement is recorded at the output reading point (end of truss structure).

In Table 2, the values of  $l$  and  $\vartheta$  that were calculated and used in order to guarantee constant relative density for each configuration are shown:

4.2.1 Hexagonal

The unit cell as well as a representation of the hexagonal topology are shown in Fig.4.

Fig. 5 and Fig. 6 show the FRF plots and the dispersion curves for the hexagonal topology. The

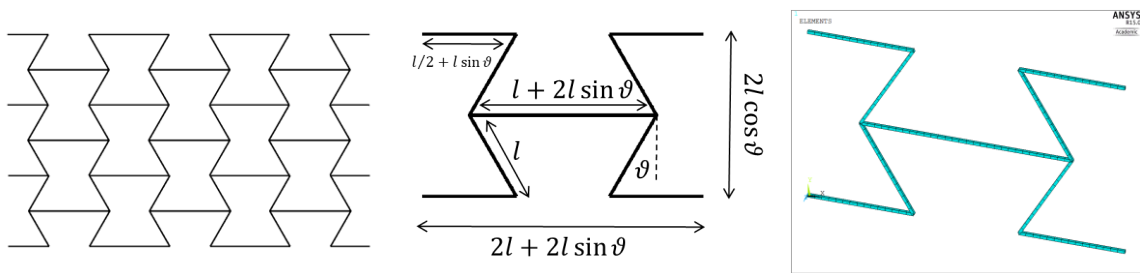


Fig. 7 Re-entrant unit cell (left) and example core (right)

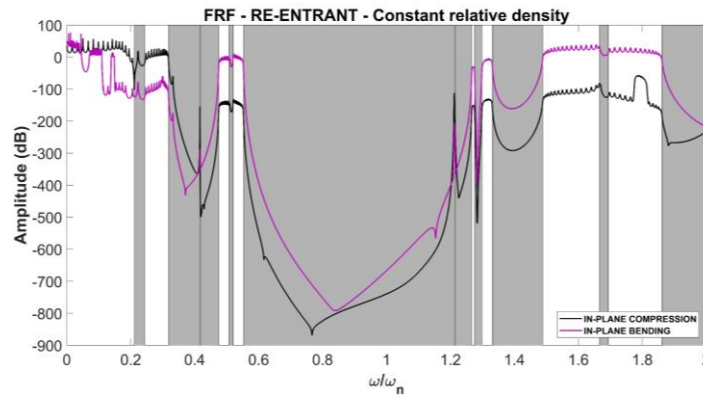


Fig. 8 FRF plot for Re-entrant topology

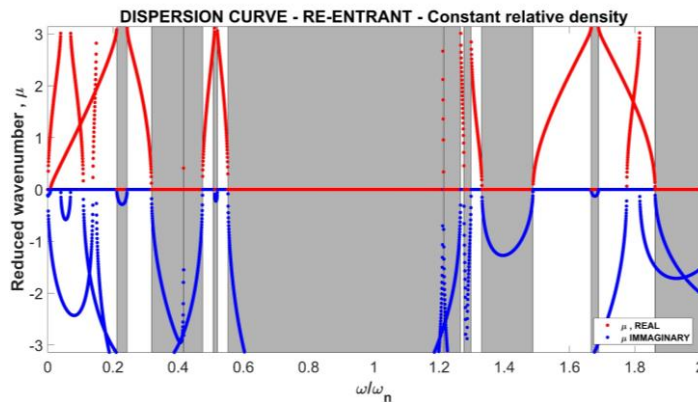


Fig. 9 Dispersion curve for Re-entrant topology

graphs are normalized according to the 1<sup>st</sup> eigenfrequency of the  $l$  beam. There is very good correspondence between dispersion curves (infinite structure) and the computed FRF plots (finite structure).

The graphs both show the presence of bandgaps around  $\omega/\omega_n = 0.3, 0.45, 0.85, 1.2$  and  $1.7$ .

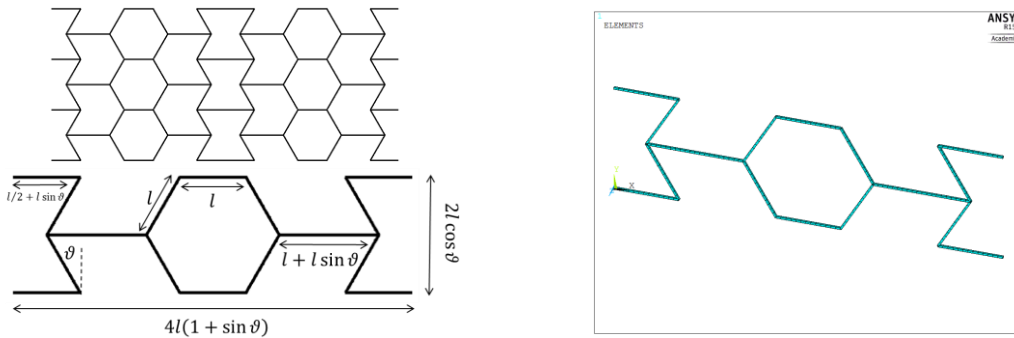


Fig. 10 AUXHEX unit cell (left) and example core (right)

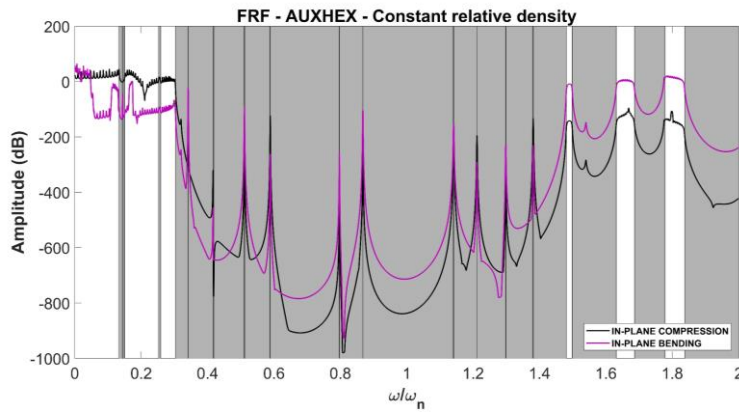


Fig. 11 Dispersion curve for Re-entrant topology

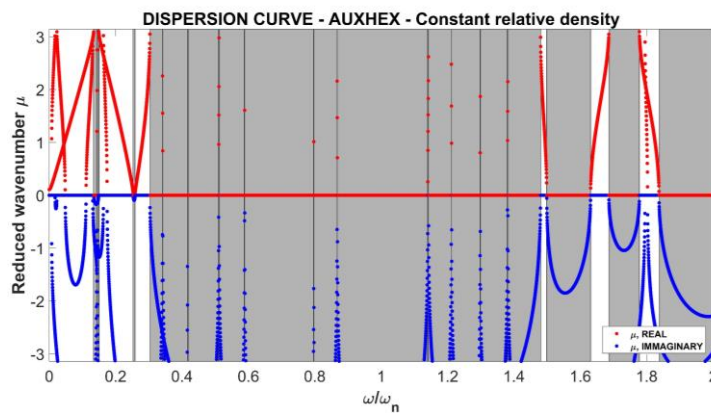


Fig. 12 Dispersion curve for AUXHEX topology

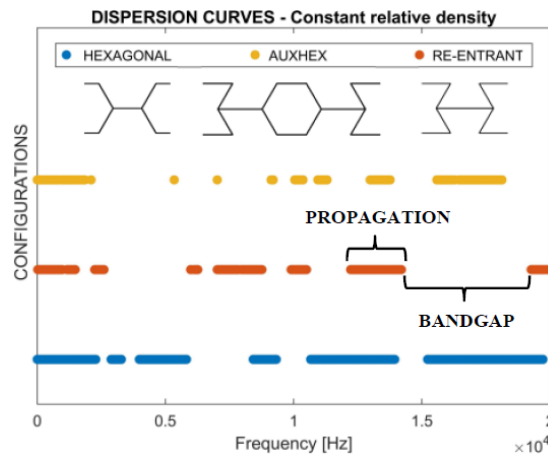


Fig. 13 Dispersion curve of the three topologies considered for the comparison

#### 4.2.2 Re-Entrant

Just as for the Hexagonal configuration, the unit cell dimensions as well as the FRF and Dispersion curves are shown in Figs.7, 8 and 9.

The graphs both show the presence of bandgaps around  $\omega/\omega_n = 0.22, 0.35, 0.45, 0.9, 1.4$  and above 1.85. Compared to the hexagonal cell core, the re-entrant possesses a wider bandgap at  $\omega/\omega_n = 0.9$ .

#### 4.2.3 AUXHEX

The AUXHEX configuration, shown in Fig.10, possesses various bandgaps. In Figs. 11 and 12, adjacent bandgaps appear in the range from  $\omega/\omega_n = 0.3$  up to 1.5. Sharp resonant peaks interrupt the continuity of a potentially very large bandgap.

#### 4.3 Dispersion curve summary

Fig. 13 is the plot of the real part of  $\mu$  (reduced wavenumber), which represents the propagative waves, over a frequency range of interest that goes from 0 Hz to 20 kHz. The blue, red and green horizontal lines represent the frequencies at which  $Re(\mu) \neq 0$  and therefore waves can freely propagate. The absence of plot translates therefore into the presence of a bandgap.

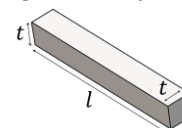
#### 4.4 Aspect ratio impact on bandgaps

A frequency response analysis was carried out varying the aspect ratio of the constituent beam to understand the impact, if any, that this parameter upon the bandgap number, width or shift. In parallel, dispersion curves were also produced, using WFEM in combination with TMM. The results from the analyses were normalised according to the 1<sup>st</sup> eigenfrequency of the smallest constituent beam of the analysed unit cell. The beam length varied from 3mm to 10 mm.

$$t = 0.2$$

$$\text{Aspect Ratio} = l/t$$

$$\omega/\omega_n = [0 - 10]$$



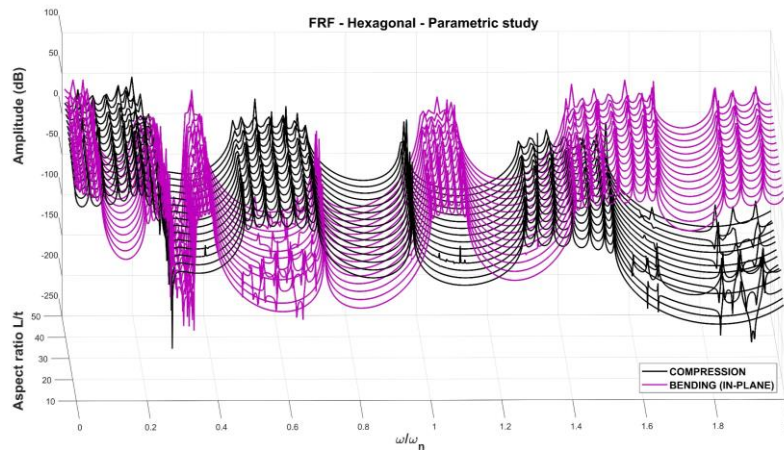


Fig. 14 FRF - Hexagonal - parametric plot

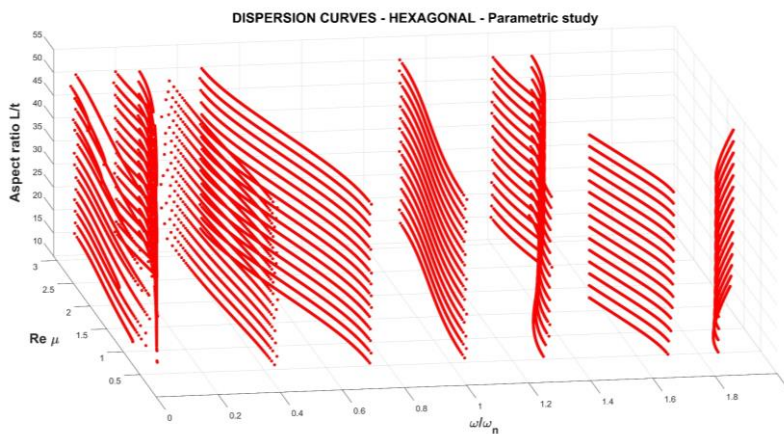


Fig. 15 Dispersion Curve - Hexagonal - parametric plot

The parametric frequency response plots and the dispersion curves for the hexagonal configuration are shown in Fig.14 and Fig. 15. By increasing  $l$  while keeping  $t$  constant, the scaling factor of the unit cell is changed, hence decreasing its overall stiffness. This is evident from the normalised parametric plots, as the dips in the FRF and the blanks in the dispersion curves are coincident for all aspect ratio considered.

#### 4.5 Bandgap inheritance

This section is focused on the results obtained for the hybrid configuration. Fig.16 shows how by repeating in space (alternating) the unit cells of the homogeneous cores, the AUXHEX configuration is reproduced.

In Fig.17, a representation of the dispersion curves and relative bandgaps produced by each homogeneous topology is proposed, while varying the aspect ratio ( $l/t$ ) and therefore to the unit cell scaling factor. The 2D plot is obtained projecting the calculated dispersion curves (like in

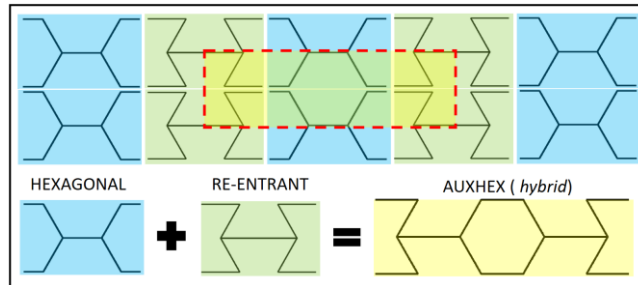


Fig. 16 Hybrid panel recreated with mixed unit cell (hexagonal and re-entrant) tessellation

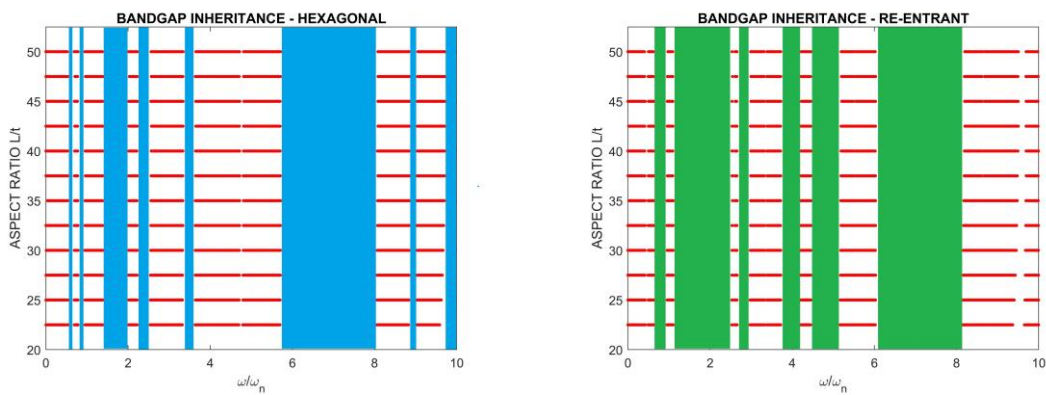


Fig. 17 Parametric dispersion curves for the Hexagonal and the Re-entrant topologies. Bandgaps shown in blue and green respectively

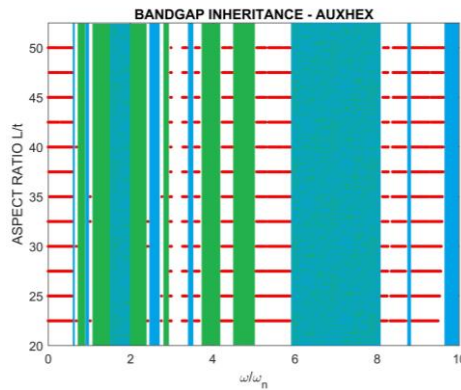


Fig. 18 Parametric dispersion curve for the AUXHEX configuration. The inherited bandgaps are shown in blue (from Hexagonal) and green (from Re-entrant)

Fig.13) over the  $\omega/\omega_n$  vs  $l/t$  plane. Each horizontal red line refers to the frequency values at which  $Re(\mu) \neq 0$  (Fig 15 may help the reader in better understanding the plot projection). The normalisation adopted underlines how the bandgap frequency range is again dependant from the unit cell scaling factor. In Fig.17 the bandgap frequency ranges are highlighted with vertical rectangles in blue (hexagonal) and green (re-entrant).

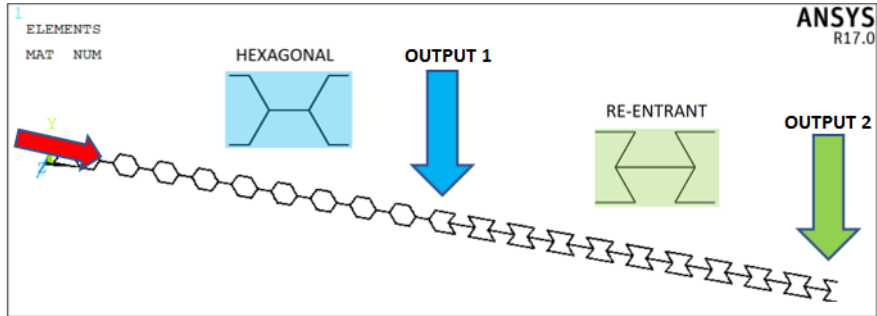


Fig. 19 New truss structure (10 hexagonal + 10 re-entrant unit cells)

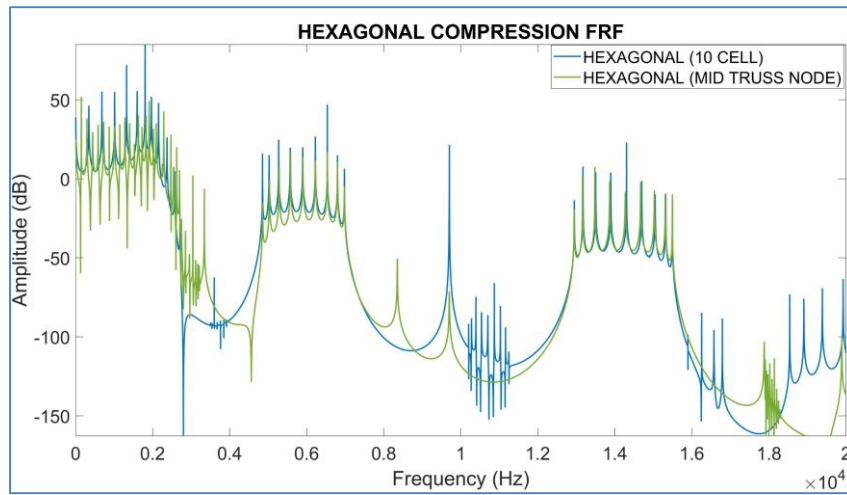


Fig. 20 Nodal output at the middle of the new truss versus the output at the end of a hexagonal core truss

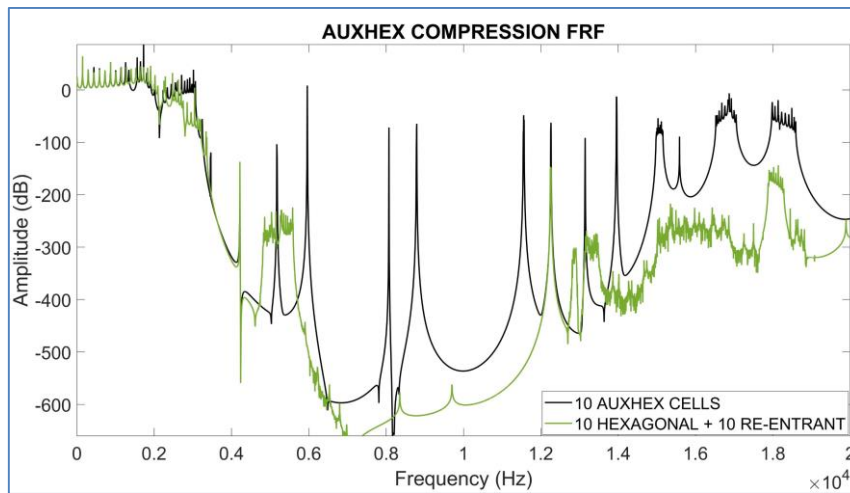


Fig. 21 Comparison between the output nodal solution at the end of the AUXHEX truss versus the output recorded at the end of the new truss (10 hexagonal + 10 re-entrant)

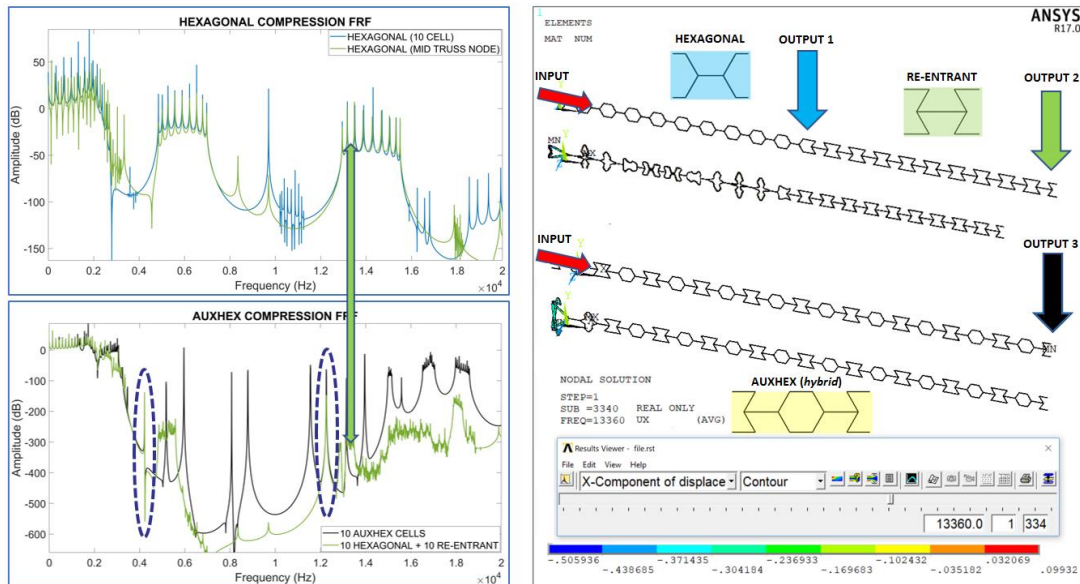


Fig. 22 Deformed shape of the new truss structure when solicited at 13360 Hz

Fig. 18 represents the bandgaps produced by the hybrid core AUXHEX. Comparing the results displayed in Fig. 17 with the ones obtained for this configuration, it seems that the capability of each type of cell (hexagonal and re-entrant), to filter waves of certain frequency ranges, is inherited by the hybrid topology. The bandgaps produced by the hexagonal and re-entrant configurations, to a certain extent, are also produced by the hybrid core and therefore inherited. This bandgap inheritance could potentially lead to bandgap-designed hybrid panels, provided that the spectral signature of the “parent” unit cells are known.

Furthermore, another simulation was carried out. A different truss structure containing a series of 10 hexagonal unit cells followed by 10 re-entrant unit cells (Fig.19) was compared with an AUXHEX truss structure of same length and relative density.

Initially, a comparison between the output amplitude reading at the end of a truss made with ten hexagonal cells and the one picked at the middle of the new truss (output 1) was made to see whether the subsequent ten re-entrant cells had any effect upon the mid-truss-node reading (blue arrow in Fig. 19). As shown in Fig. 20, no effect on the bandgap position and width was noticeable.

Consequently, to this verification, the output at the end of the new truss (output 2) was considered reliable and compared with the reading at the end of the AUXHEX truss (output 3, visible in Fig. 22). The results are plotted in Fig. 21, where the FRF trends seem to be quite close to each other.

Fig. 22 shows how by applying a compressive solicitation at 13360 Hz (frequency at which waves propagate across the hexagonal core but not trough the AUXHEX one), waves are unable to propagate until the end of the truss. This means that each unit cell from a homogeneous core is frequency-selective and hybrid cores such as the AUXHEX, inherit the filtering property of the parent-unit cells, since no matter in which way the truss is assembled, the resultant FRF maintains the bandgaps. High correspondence between the AUXHEX and the new truss FRF’s is also found at specific frequencies, circled with dashed blue lines.

## 5. Conclusions

The implementation of the Floquet-Bloch periodic boundary conditions through a transfer matrix method for 1D vibration bandgap prediction is a valuable investigation resource, since the numerical results obtained agree with the ones obtained using commercial software.

The configuration which shows the wider bandgap at lower frequencies, keeping the relative density constant, is the AUXHEX. The configuration which shows the widest bandgap within the 0-20 kHz range is the Re-entrant. Overall, the AUXHEX is the topology which shows the largest number of bandgaps in that range.

The inheritance concept, considering the 1D periodicity and compression solicitation, seems to be an interesting factor to further investigate and may lead to bandgap tailored hybrid cores. Through the opportune selection of unit cells and tessellation sequences, the vibration absorption at desired frequency ranges can be obtained.

## Acknowledgments

I would like to express all my gratitude to <sup>1</sup>Université Bourgogne Franche Comté and <sup>2</sup>University of Bristol for hosting me during my research, and to my supervisors Morvan Ouisse<sup>1</sup> and Fabrizio Scarpa<sup>2</sup>. I would also like to thank my VIPER MSCA-ITN colleagues for constant feedback, especially Marc-Antoine Campana.

This project has received funding from the European Union's Horizon 2020 research and innovation programme under Marie Curie grant agreement No 675441.

## References

- Brillouin, L. (1953), *Wave Propagation in Periodic Structures, Electric Filters and Crystal Lattices*, Dover.
- Collet, M., Ouisse, M., Ruzzene, M. and Ichchou, M.N. (2011), "Floquet–Bloch decomposition for the computation of dispersion of two-dimensional periodic, damped mechanical systems", *Int. J. Solids Struct.*, **48**(20), 2837-2848. <https://doi.org/10.1016/j.ijsolstr.2011.06.002>.
- Del Broccolo, S., Laurenzi, S. and Scarpa, F. (2017), "AUXHEX – a Kirigami inspired zero Poisson's ratio cellular structure", *Compos. Struct.*, **176.**, 433-441. <https://doi.org/10.1016/j.compstruct.2017.05.050>.
- Gibson, L.J. and Ashby, M.F. (1997), *Cellular Solids*, 2nd Ed., Cambridge University Press.
- Gonella, S. and Ruzzene, M. (2008), "Analysis of in-plane wave propagation in hexagonal and re-entrant lattices", *J. Sound Vib.*, **312**(1-2), 125-139. <https://doi.org/10.1016/j.jsv.2007.10.033>
- Hussein, M.I., Leamy, M.J. and Ruzzene, M. (2014), "Dynamics of phononic materials and structures: Historical origins, recent progress and future outlook", *Appl. Mech. Rev.*, **66**(4), 040802. <https://doi.org/10.1115/1.4026911>.
- Mace, B.R. and Manconi, E. (2008), "Modelling wave propagation in two-dimensional structure using finite element analysis", *J. Sound Vib.*, **318**(4-5), 844-902. <https://doi.org/10.1016/j.jsv.2008.04.039>.
- Mace, B.R., Duhamel, D., Brennan, M.J. and Hinke, L. (2005), "Finite element prediction of wave motion in structural waveguides", *J. Acous. Soc. Amer.*, **117**(5), 2835-2843. <https://doi.org/10.1121/1.1887126>.
- Mead, D.J. (1996), "Wave propagation in continuous periodic structures: research contributions from Southampton 1964-1995", *J. Sound Vib.*, **190**(3), 495-524. <https://doi.org/10.1006/jsvi.1996.0076>.
- Neville, R. M., Monti, A., Hazra, K., Scarpa, F., Remillat, C. and Farrow, I.R. (2014), "Transverse stiffness and strength of Kirigami zero- $\nu$  PEEK honeycombs", *Compos. Struct.*, **114**, 30-40. <https://doi.org/10.1016/j.compstruct.2014.04.001>,

- Ruzzene, M., Scarpa, F. and Soranna, F. (2003), "Wave beaming effects in two-dimensional cellular structures", *Smart Mater. Struct.*, **12**(3) 363-372.
- Scarpa, F., Ouisse, M., Collet, M. and Saito, K. (2013), "Kirigami auxetic pyramidal core: mechanical properties and wave propagation analysis in damped lattice", *J. Vib. Acoust.*, **135**(4), 041001. <https://doi.org/10.1115/1.4024433>.

CC